JCI The Journal of Clinical Investigation

Biofilm derived oxylipin 10-HOME mediated immune response in women with breast implants

Imran Khan, … , Marshall E. Kadin, Mithun Sinha

J Clin Invest. 2023. https://doi.org/10.1172/JCI165644.

Research In-Press Preview Immunology Inflammation

Graphical abstract

Biofilm Derived Oxylipin 10-HOME Mediated Immune Response in Women with Breast Implants

Imran Khan[1], Robert E. Minto[2], Christine Kelley-Patteson[3], Kanhaiya Singh[1,4], Lava Timsina[1], Lily J. Suh[1], Ethan Rinne[1], Bruce W. Van Natta[3], Colby R. Neumann[1], Ganesh Mohan[1], Mary Lester[1], R Jason VonDerHaar[1], Rana German[5], Natascia Marino[5,6], Aladdin H. Hassanein[1], Gayle M. Gordillo[1,7], Mark H. Kaplan[8], Chandan K. Sen[1,4], Marshall E. Kadin[9,10], Mithun Sinha[1*]

[1]Division of Plastic Surgery, Department of Surgery, Indiana University School of Medicine, Indianapolis, Indiana

[2]Department of Chemistry and Chemical Biology, Indiana University–Purdue University Indianapolis, Indianapolis, Indiana

[3] Meridian Plastic Surgeons, Indianapolis, Indiana

[4]McGowan Institute for Regenerative Medicine, Department of Surgery, University of Pittsburgh School of Medicine, Pittsburgh

[5]Susan G. Komen Tissue Bank at the IU Simon Comprehensive Cancer Center, Department of Medicine, Indiana University School of Medicine, Indianapolis, Indiana

[6]Division of Hematology & Oncology, Department of Medicine, Indiana University School of Medicine, Indianapolis, Indiana

[7]McGowan Institute for Regenerative Medicine, Department of Plastic Surgery, University of Pittsburgh School of Medicine, Pittsburgh

[8]Department of Microbiology and Immunology, Indiana University School of Medicine, Indianapolis, Indiana

[9]Department of Dermatology, Roger Williams Medical Center, Boston University School of Medicine, Providence, Rhode Island

[10] Department of Pathology, University of Virginia, Charlottesville, Virginia

[*] Corresponding Author: Mithun Sinha, PhD; mitsinha@iu.edu

Address:
975 W Walnut St,
Medical Research Library Building, Suite # 444A
Indiana University School of Medicine
Indianapolis, IN 46202.
Tel. 317 278 2713
Fax. 317 278 2708

Short Title: Implant biofilm mediated immune response.

Abstract

The study investigates a mechanistic link if bacterial biofilm mediated host-pathogen interaction leads to immunological complications associated with breast implant illness (BII). Over 10 million women worldwide have breast implants. In recent years, women have described a constellation of immunological symptoms believed to be related to their breast implants. The study included 178 subjects divided in three cohorts. Eighty-six patients reported symptoms consistent with BII. Control group I (non-BII, N=55) included patients with breast implants without BII symptoms but went through explantation of the breast implant. Control group II (normal tissue, N=37) was comprised of women without an implant, whose breast tissue was removed as an unrelated clinically indicated surgical procedures. We report that periprosthetic breast tissue of BII had increased abundance of biofilm and biofilm-derived oxylipin, 10-HOME. *S. epidermidis* biofilm was observed to be higher in the BII group (73.33%) compared to non-BII group (16.67%, p=0.018) and the normal group (10%, p=0.036). The oxylipin was found to be immunogenic capable of polarizing naïve $CD4^+$ T cells with a resulting Th1 subtype *in vitro* and *in vivo*. Consistently, an abundance of $CD4^+$Th1 subtype was observed in the periprosthetic breast tissue and blood of BII subjects. Mice injected with 10-HOME also had increased Th1 subtype in blood akin to BII patients and demonstrated fatigue-like symptoms. The identification of an oxylipin-mediated mechanism of immune activation induced by local bacterial biofilm associated with BII provides insight into the possible pathogenesis of implant-associated immune symptoms of BII.

Keywords

Biofilm, Implants, Host-pathogen interaction, Oxylipin, Chronic fatigue syndrome

Introduction

Breast implants were first introduced in 1962. Nearly 60 years later, their safety has continued to be controversial in the medical field, including a period of FDA-mandated restrictions on the use of silicone gel breast implants in the U.S. in the 1990s(1, 2). There are 3.3 million breast cancer survivors in the US(3) , many of whom have had breast reconstruction. Nearly 300,000 women have breast implant surgeries every year in the US(4). A subset of women with breast implants have reported a myriad of nonspecific systemic symptoms(5, 6). The symptoms described include fever, myalgias, chronic fatigue, arthralgias and other manifestations often associated with autoimmune illnesses(7-15). This constellation of symptoms related to implants has been named Breast Implant Illness (BII) or systemic symptoms associated with breast implants (SSBI).

The number of patients who opt for breast implant explantation due to complications including breast implant illness is over 30,000 annually(4). Thus, BII is a growing concern to both patients and surgeons alike with more than 10 million women worldwide currently having breast implants(7). Despite the increased concern regarding BII, existing scientific literature does not show a definite link between breast implants and autoimmune or connective tissue diseases. Several studies have reported an association of autoimmune symptoms with breast implants(8, 10-14). Symptoms have been documented to begin after placement of the implant and are often relieved by explantation (14, 16, 17). This has led patients and physicians to suspect that breast implants are the likely cause of the observed symptoms (14, 16, 17). However, studies have found silicone gel breast implants to be safe(18). Relevant to this apparent contradiction is the fact that these symptoms have been reported in subjects with other types of implants as in orthopedic arthroplasty which is typically comprised of titanium(14, 19-23). This suggests that the underlying cause of these conditions may be associated with factors other than the implant

material. Due to the rising concerns with breast implants for breast implant associated-anaplastic large cell lymphoma (BIA-ALCL) and BII, the US Food and Drug Administration (FDA) placed a black box warning on breast implants(24). Therefore, it is important to decipher the underlying molecular mechanism(s) associated with BII for a better understanding of all implant-related illnesses with systemic immunological manifestations.

Immune cells have been studied to evaluate the biocompatibility of breast implant surfaces(25-27). Earlier studies showed the presence of activated $CD4^+$ T-cells in the periprosthetic tissue of capsule/silicone implant from the biopsies recovered(28-30). T lymphocytes that were found at the implant site, had been suggested to be due to the prolonged action of *Staphylococcus* antigens which resulted in stimulation of lymphocytes leading to clonal expansion of activated T-cell(31-33). Most reports on infection and T-cell axis focused on antigen-specific T-cell responses (34, 35). Bystander activation of $CD4^+$ T cells, and the role of antigen unrelated $CD4^+$ T cells in various infections might lead to the development of autoimmune diseases but the mechanisms involved have not been identified (36, 37). Bacterial products, such as oxidized lipids or lipopolysaccharide (LPS), bind to the surface of naïve T cells and resulted in IFN-α/β secretion, which further contributed to the proliferation and expansion of heterologous polyclonal T cells(38-40).

This is the first study to investigate in depth the possible role of bacterial biofilm as one of the factors in the pathogenesis of BII through a patient-based study with a mechanistic pathway. The biofilm-derived molecule 10-HOME could be a potential therapeutic target to intervene in implant-association immunological complications.

Results

Bacterial Biofilm in Implant-Associated with BII

The study included 178 subjects divided in three cohorts. Eighty-six patients with BII manifestations were analyzed. Subjects were diagnosed with BII using clinical parameters outlined in previous studies (7-13) **(Fig. 1A)**. As a part of the diagnosis, the patients were required to complete a questionnaire **(Supplementary Table 1)**. The questionnaire screened for the commonly reported symptoms associated with BII (7-13). Implants, associated capsules, periprosthetic breast tissue and peripheral blood were collected from these subjects **(Fig. 1B-C)** as described in the Methods section. The mean age of BII patients was 48.2 years with mean duration of implant insertion of 12.89 years. Two groups were considered as controls. Control group I (non-BII, N=55) included patients with breast implants without BII symptoms but who underwent explantation of the breast implant. The mean age of non-BII patients was 53.3 years, with mean duration of implant insertion of 13.2 years. Control group II (normal tissue, N=37) was comprised of women without an implant, whose breast tissue was removed as a clinically indicated surgical procedures such as mastopexy or breast reduction. The mean age of control group II subjects was 42.17 years. The demographics of the subjects have been provided in **Supplementary Table 2**.

Bacterial biofilm was detected in implant-associated capsules through scanning electron microscopy **(Fig. 1D, Supplementary Fig. S1A)**. Though biofilm was detected in the capsules of implants from both BII and non-BII subjects, the abundance of biofilm was significantly more in the capsules of BII subjects as observed through wheat germ agglutin (WGA) assay($p=0.0036$) **(Fig 1E-F)**. The microbiological culture analyses resulted in limited or no growth of bacterial colonies (**Supplementary Table 3**). It has been reported that bacterial biofilms are difficult to detect through colony-forming assays due to their subdued metabolism (41, 42). Hence, in cases of bacterial biofilm, next generation sequencing (NGS) using the variable region of bacterial 16S rRNA gene is employed to type bacteria and determine their abundance(43). Diverse types of biofilm-forming bacteria were observed associated with

normal tissues, non-BII and BII tissues **(Fig. 1G-I)** through NGS of the 16S rRNA variable region. Most of the species identified were opportunistic bacteria associated with normal skin flora capable of forming biofilms **(Fig. 1G-I)**. Comparative ranked analyses with the normal, non-BII and BII groups revealed an increased abundance of *Staphylococcus epidermidis* in BII **(Fig. 1J, K)**. The other bacteria found in increased abundance in breast tissues of three cohorts was *Cutibacterium acnes* (previously known as *Propionibacterium acnes*). Bivariate analysis using cross-tabulation was performed between presence of biofilm and the study groups. Using the two-sample test of proportions with z-tests, *S. epidermidis* colonization was observed to be higher in the BII group (73.33%) compared to non-BII group (16.67%, p=0.018) and the normal group (10%, p=0.036). The BII group was 2.4 times more likely to have *S. epidermidis* colonization compared to the non-BII group (Odds Ratio=2.4). Similarly, when comparing with normal group, the BII group was 3.4 times more likely to have *S. epidermidis*. Both the spider and the bubble plot indicate that *S. epidermidis* was found in increased abundance in the BII group compared to normal or non-BII groups **(Fig. 1J, K)**. Within the BII group, we ranked the bacterial types using its proportion and obtained the top 5 colonizations (*C. acnes, S. epidermidis, Corynebacterium tuberculostearicum, Pseudomonas fluorescens, and Acinetobacter sp.*) **(Fig. 1I)**. We used these bacteria to examine their ranking across the groups (**Supplementary Fig. S1B**). Compared to BII, the proportion of each of these 5 bacteria colonizations were about 46% to 86% lower in the other two groups. It is to be noted that *C. acnes* was consistently the highest ranked bacterial type across groups, though the same was not true for *S. epidermidis* which was more predominant in the BII cohort (**Fig. 1J**). Increased abundance of *C. tuberculostearicum* was also found in peri-prosthetic tissue of BII samples compared to normal tissue (**Supplementary Fig. S1B**). However, the study did not observe a significant difference in abundance of *C. tuberculostearicum* between BII and non-BII cohort.

Increased Abundance of Biofilm Derived 10-HOME in BII Subjects

Previous reports identified oxylipins as molecules mediating the interaction between host and bacteria(44-46). The oxylipin (*E*)-10-hydroxy-8-octadecenoic acid (10-HOME) is formed by the bacterial oxidation of oleic acid (47)**(Fig. 2A)**. Oxylipin 10-HOME has been reported to inhibit flagellum-driven swimming and swarming motilities and stimulate the formation of bacterial biofilms *in vitro*(48). The oxylipin 10-HOME was synthesized in the laboratory in natural isotopic abundance (light) isotope and deuterated (heavy) isotope forms. The synthesized 10-HOME was validated through high-resolution mass spectrometry, thin-layer chromatography, LCMS and NMR spectroscopy **(Supplementary Fig. S2-9)**. We explored the role of 10-HOME in the association between BII-related symptoms and bacterial biofilm.

By liquid chromatography-mass spectrometry (LC-MS/MS), we observed elevated levels of 10-HOME in implant-associated periprosthetic tissue of BII compared to non-BII samples, $p<0.0001$ (**Fig. 2B-D, Supplementary Fig. S10-11**). In the age-adjusted bootstrapped analysis, BII periprosthetic tissue had 28.13 units higher levels of 10-HOME relative to non-BII subjects. A positive correlation was observed between bacterial abundance and 10-HOME concentration in periprosthetic tissue of BII subjects **(Fig. 2E)**. For every unit increase in 10-HOME levels, the percent bacterial abundance increased by 0.34 units ($p=0.022$). Similar correlation was observed in BII subjects with *Staphylococcus epidermidis* **(Fig. 2F)**. To determine if *S. epidermidis* was capable of synthesizing 10-HOME, it was cultured *in vitro* in basic M9 salt media with oleic acid as a source of carbon. Formation of 10-HOME was detected using gas chromatography-mass spectrometry and LC-MS/MS **(Fig. 2G, Supplementary Fig. S1C-E)**. In addition to *S. epidermidis*, we tested 7 bacterial species (from three cohorts, **Fig 1G-I**), 4 didn't produce 10-HOME (at very low or undetectable levels) through LC-MS/MS. Three (including *S. epidermidis*) produced 10-HOME **(Supplementary Fig. S1F)**. The other two *Pseudomonas fluorescens* and *Acinetobacter sp*. were also present in non BII and normal breast microflora and had a lower abundance **(Fig. 1G-I).** Oxylipins have been reported to cause immune

activation *via* alteration in expression of transcripts in immunological pathways(49). We subsequently explored the global transcriptome in the BII cohort.

Comparative Transcriptomic and Molecular Pathway Analyses of BII Subjects

To explore the mechanisms underlying BII, we performed bulk RNA-Seq with a depth of 30 million reads on periprosthetic tissue from BII and non-BII subjects (GSE178425) and compared it to the RNA-Seq database (GSE164641) of normal breast tissue (anatomical similar location to periprosthetic breast tissues). Findings from normal breast tissue (N=34), non-BII (N=16) and BII (N=24) revealed differential expression of 16428 transcripts between normal breast tissue *vs* periprosthetic tissue (non-BII and BII) (**Fig. 3A**). This implied that placement of the implant had a profound effect on the alteration of the local (periprosthetic breast tissue) transcriptome (**Fig. 3A**). Upon comparison between BII *vs* non-BII cohorts, 2878 genes were differentially expressed (**Fig 3A, Supplementary Fig. S12**). We observed altered gene expression related to adaptive T cell response in BII subjects compared to non-BII and normal subjects (**Fig. 3B-E**, **Supplementary Fig. S12)**. Molecular network analysis also suggested the involvement of T cell pathway **(Fig. 3B)**. Canonical pathways identified through Ingenuity Pathway Analysis (IPA)™ revealed that the majority of the differentially expressed genes associated with transcripts belong to Th1 pathway (**Supplementary Fig. S12**). Increased *CD36* (fatty acyl translocase) (**Fig. 3C**) and Th1 responsive genes including the Th1 specific transcription factor, *TBET (TBX21)* were observed in the BII cohort (**Fig. 3D-E**). Th1 cells are associated with an auto-immune response in multiple illnesses including rheumatoid arthritis. CD36 is a fatty acyl translocase; its level is upregulated when uptake of fatty acids (normal or oxidized) is required.

Abundance of $CD4^+$ Th1 Cells in Implant-Associated Tissue of BII Subjects

In agreement with the RNA-Seq data, periprosthetic breast tissue associated with the implant of BII subjects showed an increase of $CD4^+CD36^+$ cells **(Fig. 4A)**. The $CD4^+$ T cells associated

with BII subjects were T-BET$^+$ compared to that of non-BII and normal breast tissues as observed through immunohistochemistry **(Fig. 4B)**. The T-BET transcription factor is critical in Th1 subtype determination. Because BII is reported as a systemic immune manifestation, peripheral blood of BII and non-BII subjects was analyzed for CD4$^+$ T cells (Th1, Th2, Th9 and Th22) using flow cytometry and (Th1, Th2, Th9, Th17, Th22, and Treg) using mass cytometry time of flight (CyTOF). An increase of Th1 cells was observed in BII subjects as measured through flow cytometry using T-BET **(Fig. 4C, Supplementary Figure S13)** and CD183/CXCR3 (Th1 cell markers) **(Fig. 4D, Supplementary Figure S13),** compared to non BII and normal subjects. No significant difference was observed in other Th subtypes including Th2 (CD194, GATA3), Th9 or Th22 (CD196) between BII subjects and non-BII subjects **(Supplementary Figure S13, Supplementary Fig. S15A-C)**. The following human cell lines were used as positive control for validation of surface antigens: Mac2A for CD183 (50), Mac2B for CD194(50) and TLBR1 for CD196(51) **(Supplementary Fig. S14A-C)**. The increase of the Th1 cytokine IFN-γ (**Supplementary Fig. S13D, F**) in breast tissue and serum of BII subjects and relatively unchanged levels of Th2 cytokine IL-10 (**Supplementary Fig. S13E, G**) further supports specific Th1 activation.

Assessment through mass cytometry (CyToF) showed that the T cells isolated from the peripheral blood of BII subjects exhibited an increase of Th1 phenotype (**Fig. 4E-F, Supplementary Fig. S15A-C, Supplementary Figure S16**). Mass cytometry by time of flight (CyTOF) analyses did not reveal any significant difference in Th2, Th9, Th22, Th17 and Treg populations between the three cohorts (**Supplementary Figure S16**).

However, these results do not definitively establish that 10-HOME led to CD4$^+$Th1 cell induction or that 10-HOME can lead to CD36 upregulation. Thus, we studied the effect of 10-HOME on human primary naïve CD4$^+$ T cells.

Oxylipin 10-HOME Polarizes Naïve CD4$^+$ T Cells to Th1 Subtype *in vitro*

In order to study the effect of 10-HOME on T cells, naïve CD4$^+$ T cells (isolated from healthy human peripheral blood mononuclear cells) were treated with 100 μM 10-HOME for 48h. Naïve CD4$^+$ T cells are not antigen challenged and thus are not committed to any specific subtype. Increased CD36 expression was observed in the 10-HOME-treated CD4$^+$ T cells through immunocytochemistry **(Fig. 5A)**, flow cytometry **(Fig. 5B)** and quantitative real time PCR **(Fig. 5H)** indicative of the 10-HOME-mediated induction of CD36. Polarization to Th1 subtype occurred in the presence of 10-HOME as observed through immunocytochemistry **(Fig. 5C)**, flow cytometry **(Fig. 5D)**, and quantitative real time PCR **(Fig. 5I)**. The CD4$^+$ cells exhibited increased expression of T-BET (a transcription factor activated during the polarization of naïve T cells to Th1 subtype) (**Fig. 5C, 5I, Supplementary Fig. S17A**), CD183/ CXCR3 (CD4$^+$ Th1 cell marker) (**Fig. 5D**), and Th1 secreted pro-inflammatory cytokine IFN-γ through ELISA (**Fig. 5E**). The CD183$^+$ Th1 cells exhibited increased abundance of CD36 marker (**Supplementary Fig. S17B**). The other subtypes of CD4$^+$ T cells (Th2, Th9 and Th22) assayed did not exhibit any statistically significant increase in post 10-HOME treatment on naïve CD4$^+$ T cells. Th2 cells were assayed using surface marker CD194/CCR4 (**Supplementary Fig. S17C**), transcription factor GATA3 (**Supplementary Fig. S17D**) and anti-inflammatory cytokines IL 4 and IL10 (**Fig. 5F-G**). Th9 and Th22 cells were assayed using surface marker CD196/CCR6 (**Supplementary Fig. S17E**). CD4 T cells were exposed to the media obtained from *S. epidermidis* treated cells. Upon analyzing the supernatant collected from the co-culture, we observed polarization to the Th1 subset (increased abundance of CD183$^+$ cells). However, using the bacterial supernatant increased CD194$^+$ cells, corresponding to Th2 subtype was also observed. No change in CD196 (Th9, Th22 marker) was observed. Bacterial supernatant is heterogenous (unlike 10-

HOME only). The other factors present in the supernatant may be triggering the polarization of CD194 expressing along with CD183 expressing T cells (**Supplementary Fig. S18**).

Elevated $CD4^+$ Th1 and Fatigue-like Symptoms in Mice Administered with 10-HOME

To evaluate if 10-HOME can induce Th1 cells *in vivo*, we administered 10-HOME into the abdominal mammary fat pad of C57BL/6 mice (**Fig. 6A**). The timeline of *in vivo* murine model has been provided (**Fig. 6B**). Two concentrations, a higher (6.5 mg/kg body weight for 10 days, based on existing oxylipin reports (52) and a lower concentration (0.5 mg/kg for 30 days) of 10-HOME was administered at times specified into the abdominal mammary fat pad of C57BL/6 mice. An increased abundance of $CD4^+$ Th1 ($CD183^+$) cells was found in the murine blood in both protocols following administration of 10-HOME (**Fig. 6C, Supplementary Figure S19-20**). In line with the observation, an increase of $Tbet^+$ $CD4^+$ cells were observed in the murine cohort administered with 10-HOME (**Fig. 6D, Supplementary Figure S19-20**). Other subtypes of $CD4^+$ T cells (Th2) **(Fig. 6E, Supplementary Fig. S19A, Supplementary Figure S20)** and Th9 and Th22 (**Supplementary Fig. S19B, Supplementary Figure S20**) were not statistically different. Similar administration of 10-HOME in ZsGreen mice with *Tbet/Tbx21* promoter (Tbet-ZsGreen reporter) led to increase of ZsGreen+ cells (**Supplementary Fig. S19C-D**). This implied activation of Th1 responsive *Tbet/Tbx21* promoter in presence of 10-HOME. To simulate the fatigue-like symptoms of women with BII, we assessed exercise tolerance of mice through endurance test using murine treadmill. Fatigue was quantified by two parameters (a) the number of times stopped and (b) the number of instances that aversive stimulation (contact with shock grid) was required. Animals with 10-HOME exhibited increased stops **(Fig. 6F-G, Supplementary video SV1)** and contact with shock grid **(Fig. 6H)**.

$CD4^+$ T Cells in Reaction with 10-HOME Polarizes Macrophages to M1 Phenotype

There is a dynamic interaction of macrophages and T cells during antigen presentation(53, 54). Through an assessment of peri-prosthetic tissue by bulk RNA-Seq analyses, there was an increase of genes associated with M1 macrophage phenotype in the BII cohort compared to non-BII and normal tissues (**Fig. 7A, Supplementary Fig. S21A**). Assessment of the abdominal mammary fat pad from mice administered with 10-HOME showed an increased abundance of resident macrophages of M1 phenotype (**Fig. 7B-D, Supplementary Fig. S22, Supplementary Fig. S23**). In adipose tissue, adipose cells filled with lipid occupy most of the tissue. Other cells are present in borders of adipose cells. Cells co-stained with DAB (antibody) and hematoxylin (nucleus) were used for analyses of macrophage phenotype (**Supplementary Methods**). Other than macrophages, the 10-HOME treated animal's adipose tissue exhibited increased infiltration of cells as observed through presence of more hematoxylin positive nuclei those that were not antibody stained. This was expected and in line with data presented for infiltration of T cells in the adipose tissue. To determine if the observation of M1 macrophage polarization is epi-phenomenon or influenced by T cells in reaction to 10-HOME, we performed trans-well assay. T-cells pre-treated with 10-HOME polarized PBMC derived M0 macrophages to the M1 phenotype suggested a direct effect of T-cells (**Fig. 7E-G, Supplementary Fig. S21B**).

Discussion

Bacterial biofilms have been implicated to cause gastric cancer by *Helicobacter pylori*(55), colon cancer(56), breast implant-associated anaplastic large cell lymphoma (BIA-ALCL) and chronic inflammation(57, 58). The factors that involve interplay between host and pathogen are influenced by the micro-environmental niche where the bacteria reside(42, 59-61). Breast implants provided a conducive surface for the adherence and growth of bacterial biofilms(62). Many bacteria belonging to the normal microflora of the body have been reported to form

bacterial biofilms(63). The observation in this study of increased abundance of bacterial biofilm comprised of *Staphylococcus epidermidis* through NGS, in implant-associated tissue of BII patients relative to controls was thus critical in understanding of a potential etiology of BII. It is to be noted that while this study was being performed, anecdotal evidence of *S. epidermidis* with BII was reported by Lee *et al* (64). *S. epidermidis* has been reported to be one of the main reasons for post-surgical implant failure and infection(31).

Implant material bioengineering including that of breast implants have substantially improved over time(65). There is a general perception of breast implant-associated complications like BIA-ALCL to be linked with textured implants(66). However, this study and others have recognized that BII related immunological complications manifest irrespective of implant type(11, 64). This may be linked to the collagen capsule around the implant, which serves as the substratum for biofilm adherence and growth. Both smooth and textured implants form this capsule. The current study was not able to conclude any bias towards a specific type of implant.

The practice of capsulectomy for subjects diagnosed with BII in addition to implant removal further lends credence to the biofilm hypothesis(67). A recent report of 248 subjects described better outcomes post-capsulectomy in BII patients and reported an abundance of *Staphylococcus sp*. in their breast tissue(68).

Studies by us and others have reported the ability of bacteria to co-opt host lipids to form pathogenic biofilm(61, 69). The oxidation of fatty acids is one of the main biochemical reactions in the synthesis of lipid mediators. The oxygenation of unsaturated fatty acids leads to the formation of oxylipins. Although fatty acids are mostly found as triglycerides, the action of bacterial lipases result in the availability of free fatty acids. These fatty acids can then be oxidized by bacterial dioxygenases (DOX) and lipoxygenases (LOX) to form oxylipins. When oleic acid is used as a bacterial substrate, it is oxidized to (*E*)-10-hydroxyoctadecenoic acid (10-

HOME). Notably, the adipose tissue found in breast is rich in oleic acid containing lipids(70). The oxylipin 10-HOME has been reported to promote establishment of bacterial biofilms *in vitro*(48). The increased abundance of 10-HOME detected in our study associated with breast tissues of BII subjects thus suggests that breast microflora may interact with breast lipids promoting the formation of bacterial biofilms. Oxylipins are also known to be immuno-modulatory. It has been reported that 12,13-DiHOME derived from oxidation of linoleic acid led to the reduction of regulatory T cells (Tregs), impeded immune tolerance and promoted childhood atopy and asthma(49). This study reports that elevated levels of 10-HOME produced by bacterial biofilms led to immune cell activation as observed through *in vitro* and *in vivo* murine studies.

Immunological manifestations of BII are systemic. Implant-associated periprosthetic breast tissue from BII subjects revealed an increase of Th1 pathway activation-related transcripts via RNA-Seq. In support of our findings, a similar pathological activation of $CD4^+$ Th 1 cells by microbial biofilm has been previously reported(71). $CD4^+$ T cells play an important role in the pathogenesis of chronic systemic inflammatory autoimmune diseases such as multiple sclerosis, diabetes and rheumatoid arthritis(72). Previous studies have shown *S. epidermidis* skewed T-cell response toward a balance that allowed a stalemate between the host and the pathogen, in which the infection can become chronic (73-75). Oxylipins, such as prostaglandins and leukotrienes, had been extensively studied for their immunomodulatory effects (76). Prostaglandin E2 (PGE2) had been shown to promote the differentiation of naive CD4 T cells into regulatory T cells (Tregs) and skew the immune response towards immunosuppression (77). On the other hand, leukotrienes have been associated with promoting inflammation and Th2-type responses (78, 79). Other oxylipins, such as lipoxins and resolvins, have been found to exert anti-inflammatory and pro-resolving effects (80, 81). The effects of oxylipins on T cell

skewing can be complex and context dependent. The presence of other cytokines, cell types, and the specific microenvironment could influence the outcome of T cell responses to oxylipin.

Oxidized lipids have been associated with pain and inflammatory conditions(82). Pain reported as arthralgia and myalgia is common in BII. We identified an increased presence of $CD4^+$ Th1 cells in the breast tissue and peripheral blood of BII subjects. Findings of this study demonstrate that 10-HOME could polarize naïve $CD4^+$ T cells towards Th1 subtype *in vitro* and *in vivo*. An increased abundance of the transcription factor Tbet, which is required for Th1 polarization, was identified post 10-HOME treatment. The polarization to Th1 subtype was also supported by the observation of increased expression of pro-inflammatory cytokine IFN-γ, secreted by Th1 cells. Systematic analyses using mass cytometry revealed an increased abundance of Th1 subtype. The study did not show significant polarization towards Th2, Th9, Th17, Th22, and T-reg cell subtypes.

To correlate the association of 10-HOME with activation of $CD4^+$ T cells *in vivo*, mice were administered with two different concentrations of 10-HOME in their mammary fat pad. An increase of $CD4^+$ Th1 cells in peripheral circulation in 10-HOME administered mice was observed in both cases. These observations help to explain the increased abundance of $CD4^+$ Th1 cells in the BII subjects. Animals administered with 10-HOME exhibited fatigue-like symptoms as assessed using endurance test.

Taken together, we investigated the biofilm hypothesis of breast implant illness through a host-pathogen interaction. Implant-associated complications are poorly understood. These may be multifactorial. This work may be viewed as a first step in laying fundamental molecular mechanistic groundwork, towards an understanding of a possible etiology for BII mediated via host-biofilm interaction. The breast microenvironment led to formation of the biofilm-derived lipid metabolite 10-HOME from host oleic acid. The 10-HOME thus formed led to preferential

activation of $CD4^+$ Th1 cells *in vitro* and *in vivo*. The study provides the first evidence of a possible role of biofilm-derived 10-HOME inducing an immunological response in patients with BII. Intervention to formation of biofilm-induced 10-HOME molecule could serve as possible therapeutic strategy to relieve patient symptoms in BII. Additionally, in light of the reports of biofilm association with metal implants such as orthopedic arthroplasty, this study provides a possible explanation of similar immunological responses reported in subjects with those implants(19-23). The findings of this study suggest that management of biofilm can help to increase the safety and long-term use of surgical implants. Further research needs to be conducted to elucidate if other biofilm-forming bacterial species are involved in the pathogenesis of BII. Also, the role of oxidized lipid products needs to be researched in a similar context. This study is an important step towards a mechanistic explanation of a multifactorial problem of BII which is at present limited primarily to epidemiological studies with little research on molecular mechanism which could open paths to therapeutic interventions.

Materials and Methods

(*Methods and Statistical analyses are detailed in Supplementary Information*)

ELISA. Cell-free supernatants were collected and stored at −80°C. ELISAs for IFN-γ, IL4 and IL10 were performed using DuoSet kits (R&D Systems) as per manufacturer's protocol.

Bacterial strains. *Staphylococcus epidermidis* (Winslow and Winslow) Evans (ATCC® 35984) *Pseudomonas fluorescens* (ATCC® 135925)*, Acinetobacter sp* (ATCC® 49139)*, Sphingomonas sp* (ATCC® 31461)*, Enterobacter cloacae* (ATCC® 13047)*, Cutibacterium acnes* (ATCC® 6919)*, Cornyebacterium tuberculostearicum* (ATCC® *35692),* were grown on tryptic soy agar plate at 37°C and thereafter were sub-cultured in M9 media supplemented with oleic acid 1% v/v for LC-MS/MS analyses.

10-HOME administration in mice. At 9 to 10 weeks of age, female mice were anesthetized with isoflurane. Two protocols (high and low dose) were followed. In high dose, five injections of 10-HOME (6.5 mg/kg body weight) were performed with a 27 G needle for 5 days to the abdominal mammary fat pad of mice. In low dose, 0.5 mg of 10-HOME/kg body weight was injected for 30 days to the abdominal mammary fat pad of mice. Blood was harvested for subsequent analyses.

RNA-Seq: The RNA-Seq data have been deposited in the NCBI Gene Expression Omnibus (accession# GSE178425 for periprosthetic breast tissue BII and non-BII subjects and GSE164641 for normal breast tissue).

Quantification and statistical analysis. The distribution of the increased abundance of Th subtypes were evaluated for normality using Shapiro-Wilk test and Q-Q plot. Descriptive statistics by groups (BII, non-BII, and normal) were calculated using mean (standard deviation) for normally distributed data and median (inter-quartile range) for those deviating from normality. Two-sample test of proportions with two-tailed z-tests were used to analyze the hypothesis that the proportion of different type of bacteria in the BII group was significantly different than the proportion of the biofilm infection in the non-BII and normal group. Non-parametric bivariate analyses were performed using the Kruskal-Wallis test followed by Dunn's test for pairwise comparisons with Benjamini-Hochberg multiple testing adjusted p-values to minimize the false discovery rate. A p-value less than 0.05 was considered statistically significant.

Human subjects. Subjects participating in the study included three cohorts. The first group consisted of patients diagnosed with symptoms of BII. Two additional groups of subjects were evaluated as controls, implanted patients without symptoms of BII (non-BII) and non-implanted breast tissue (normal). Subjects were diagnosed for BII using a clinical evaluation process that

included a detailed medical history interview, a review of a comprehensive symptom inventory (**Supplementary Table 1**) and a physical examination as outlined in previous BII studies (7-13). Demographic characteristics of the patients are presented in **Supplementary Table 2**. All human studies and subject questionnaire were approved by the Indiana University School of Medicine Institutional Review Board IRB# 2003674175. Declaration of Helsinki protocols was followed, and patients gave their written informed consent.

Animals. All animal (mice) experiments were approved by the Indiana University School of Medicine Institutional Animal Care and Use Committee (SoM-IACUC) under protocol 19102 and 22029 - *Murine model of breast implant diseases*. Animals were housed under a 12 h light–dark cycle with food and water *ad libitum*.

Data availability

Supporting data values for bar and line graphs have been exhibited as supplementary supporting data values excel sheet.

Author Contributions

MS, IK and AHH conceived and designed the work. IK, REM, CKP, KS, LT, LJS, ER, BWV, CRN, GM, ML, RJV, RG and NM participated in the data acquisition and analyses. MS, REM, IK, CKP, AHH and MEK wrote the manuscript. MS, REM, CKS, GMG, MHK, MEK reviewed the manuscript.

Acknowledgments

This work was supported by the US National Institutes of Health (NIH) grants R01AI165958 and R21AI171932 to MS, Plastic Surgery Foundation grant 831458 to MS. The content is solely the responsibility of the authors and does not necessarily represent the official views of the National Institutes of Health or other sponsors. Department of Defense W81XWH2110135, and NIH K08HL167164 grants to AHH. The protected research time through these grants helped AHH to contribute to the study. The US National Institutes of Health grants NIH NR015676 to GG and CKS; NIH R01DK125835 to CKS. We thank Dr. Jinfang Zhu (Senior Investigator, NIH/NIAID) for kindly providing Tbet-ZsGreen mice. Mass Cytometry findings reported were performed in the Massachusetts General Hospital (MGH) Department of Pathology Flow and Mass Cytometry Research Core, which obtained support from the NIH Shared Instrumentation program with grants 1S10OD012027-01A1, 1S10OD016372-01, 1S10RR020936-01, and 1S10RR023440-01A1. We would like to thank the Center for Genomics and Bioinformatics at Indiana University, Bloomington, for their assistance with RNA-Seq experiments. The authors acknowledge Core Services for SEM at INDI Core, Indiana University Purdue University Indianapolis. We thank the Metabolite Profiling Facility, Purdue University, West Lafayette. RNA-Seq data of normal breast tissue was generated using samples from the Susan G. Komen Tissue Bank at the IU Simon Comprehensive Cancer Center. We thank contributors who collected samples used in this study, as well as the donors and their families. We thank Dr. Alan Epstein, Keck School of Medicine, University of Southern California for his kind donation of the breast implant-associated anaplastic large cell lymphoma (BIA-ALCL), T cell line TLBR1. We thank Mahmed Shabbar Ali for his help on Adobe Illustrator. BioRender software was used to make the graphical abstract. We thank Luci Hulsman for her help with the graphical abstract.

Declaration of interests

The authors declare no competing interests.

References

1. Bondurant S, Ernster V, and Herdman R. *Safety of Silicone Breast Implants*. Washington (DC): The National Academies Press; 1999.
2. FDA. FDA Update on the Safety of Silicone Gel-Filled Breast Implants: Center for Devices and Radiological Health, U.S. Food and Drug Administration 2011.
3. Breast Cancer Facts. *National Breast Cancer Foundation.* 2020.
4. Surgeons ASoP. In: https://www.plasticsurgery.org/news/plastic-surgery-statistics ed. plasticsurgery.org: American Society of Plastic Surgeons; 2019.
5. Fryzek JP, Signorello LB, Hakelius L, Feltelius N, Ringberg A, Blot WJ, et al. Self-reported symptoms among women after cosmetic breast implant and breast reduction surgery. *Plast Reconstr Surg.* 2001;107(1):206-13.
6. Maijers MC, de Blok CJ, Niessen FB, van der Veldt AA, Ritt MJ, Winters HA, et al. Women with silicone breast implants and unexplained systemic symptoms: a descriptive cohort study. *Neth J Med.* 2013;71(10):534-40.
7. ASAPS. Breast Implant Illness - Frequently Asked Questions/Talking Points. *https://wwwsurgeryorg/sites/default/files/BreastImplantIllness_8-21-2019_FINALpdf*. 2019.
8. Balk EM, Earley A, Avendano EA, and Raman G. Long-Term Health Outcomes in Women With Silicone Gel Breast Implants: A Systematic Review. *Ann Intern Med.* 2016;164(3):164-75.
9. Coroneos CJ, Selber JC, Offodile AC, 2nd, Butler CE, and Clemens MW. US FDA Breast Implant Postapproval Studies: Long-term Outcomes in 99,993 Patients. *Ann Surg.* 2019;269(1):30-6.

10. Khoo T, Proudman S, and Limaye V. Silicone breast implants and depression, fibromyalgia and chronic fatigue syndrome in a rheumatology clinic population. *Clin Rheumatol.* 2019;38(5):1271-6.
11. Lee IM, Cook NR, Shadick NA, Pereira E, and Buring JE. Prospective cohort study of breast implants and the risk of connective-tissue diseases. *Int J Epidemiol.* 2011;40(1):230-8.
12. Singh N, Picha GJ, Hardas B, Schumacher A, and Murphy DK. Five-Year Safety Data for More than 55,000 Subjects following Breast Implantation: Comparison of Rare Adverse Event Rates with Silicone Implants versus National Norms and Saline Implants. *Plast Reconstr Surg.* 2017;140(4):666-79.
13. Watad A, Rosenberg V, Tiosano S, Cohen Tervaert JW, Yavne Y, Shoenfeld Y, et al. Silicone breast implants and the risk of autoimmune/rheumatic disorders: a real-world analysis. *Int J Epidemiol.* 2018;47(6):1846-54.
14. Suh LJ, Khan I, Kelley-Patteson C, Mohan G, Hassanein AH, and Sinha M. Breast Implant-Associated Immunological Disorders. *J Immunol Res.* 2022;2022:8536149.
15. Glicksman C, McGuire P, Kadin M, Barnes K, Wixtrom R, Lawrence M, et al. Longevity of Post-Explantation Systemic Symptom Improvement and Potential Etiologies: Findings From the ASERF Systemic Symptoms in Women - Biospecimen Analysis Study: Part 4. *Aesthet Surg J.* 2023.
16. de Boer M, Colaris M, van der Hulst R, and Cohen Tervaert JW. Is explantation of silicone breast implants useful in patients with complaints? *Immunol Res.* 2017;65(1):25-36.
17. Peters W, Smith D, Fornasier V, Lugowski S, and Ibanez D. An outcome analysis of 100 women after explantation of silicone gel breast implants. *Ann Plast Surg.* 1997;39(1):9-19.

18. Tanne JH. FDA approves silicone breast implants 14 years after their withdrawal. *BMJ.* 2006;333(7579):1139.
19. Alijotas-Reig J, Esteve-Valverde E, Gil-Aliberas N, and Garcia-Gimenez V. Autoimmune/inflammatory syndrome induced by adjuvants-ASIA-related to biomaterials: analysis of 45 cases and comprehensive review of the literature. *Immunol Res.* 2018;66(1):120-40.
20. Greenland S, and Finkle WD. A case-control study of prosthetic implants and selected chronic diseases in Medicare claims data. *Ann Epidemiol.* 1998;8(5):319-26.
21. Laing TJ, Schottenfeld D, Lacey JV, Jr., Gillespie BW, Garabrant DH, Cooper BC, et al. Potential risk factors for undifferentiated connective tissue disease among women: implanted medical devices. *Am J Epidemiol.* 2001;154(7):610-7.
22. Mellemkjaer L, Friis S, McLaughlin JK, Thomsen BL, Kjoller K, Hogsted C, et al. Connective tissue disease after hip and knee implant surgery. *Scand J Rheumatol.* 2001;30(2):82-6.
23. Signorello LB, Ye W, Fryzek JP, Blot WJ, Lipworth L, McLaughlin JK, et al. A nationwide followup study of autoimmune and connective tissue disease among hip and knee implant patients. *J Long Term Eff Med Implants.* 2002;12(4):255-62.
24. FDA. Breast Implants - Certain Labeling Recommendations to Improve Patient Communication 2020.
25. Maimaiti Z, Li Z, Xu C, Fu J, Hao LB, Chen JY, et al. Host Immune Regulation in Implant-Associated Infection (IAI): What Does the Current Evidence Provide Us to Prevent or Treat IAI? *Bioengineering-Basel.* 2023;10(3).
26. Khatoon Z, McTiernan CD, Suuronen EJ, Mah TF, and Alarcon EI. Bacterial biofilm formation on implantable devices and approaches to its treatment and prevention. *Heliyon.* 2018;4(12):e01067.

27. Meza Britez ME, Caballero Llano C, and Chaux A. Periprosthetic breast capsules and immunophenotypes of inflammatory cells. *Eur J Plast Surg.* 2012;35(9):647-51.
28. Duvic M, Moore D, Menter A, and Vonderheid EC. Cutaneous T-Cell Lymphoma in Association with Silicone Breast Implants. *J Am Acad Dermatol.* 1995;32(6):939-42.
29. Taylor CR, Siddiqi IN, and Brody GS. Anaplastic Large Cell Lymphoma Occurring in Association With Breast Implants: Review of Pathologic and Immunohistochemical Features in 103 Cases. *Appl Immunohisto M M.* 2013;21(1):13-20.
30. Adrada BE, Miranda RN, Rauch GM, Arribas E, Kanagal-Shamanna R, Clemens MW, et al. Breast implant-associated anaplastic large cell lymphoma: sensitivity, specificity, and findings of imaging studies in 44 patients. *Breast Cancer Res Treat.* 2014;147(1):1-14.
31. Oliveira WF, Silva PMS, Silva RCS, Silva GMM, Machado G, Coelho L, et al. Staphylococcus aureus and Staphylococcus epidermidis infections on implants. *J Hosp Infect.* 2018;98(2):111-7.
32. Nguyen V, Huggins RH, Lertsburapa T, Bauer K, Rademaker A, Gerami P, et al. Cutaneous T-cell lymphoma and Staphylococcus aureus colonization. *J Am Acad Dermatol.* 2008;59(6):949-52.
33. Fujii K. Pathogenesis of cutaneous T cell lymphoma: Involvement of Staphylococcus aureus. *J Dermatol.* 2022;49(2):202-9.
34. van Aalst S, Ludwig IS, van der Zee R, van Eden W, and Broere F. Bystander activation of irrelevant CD4+ T cells following antigen-specific vaccination occurs in the presence and absence of adjuvant. *PLoS One.* 2017;12(5):e0177365.
35. Lee HG, Cho MZ, and Choi JM. Bystander CD4(+)T cells: crossroads between innate and adaptive immunity. *Exp Mol Med.* 2020;52(8):1255-63.
36. Lee H, Jeong S, and Shin EC. Significance of bystander T cell activation in microbial infection. *Nat Immunol.* 2022;23(1):13-22.
37. Boyman O. Bystander activation of CD4+ T cells. *Eur J Immunol.* 2010;40(4):936-9.

38. Tough DF, Sun S, and Sprent J. T cell stimulation in vivo by lipopolysaccharide (LPS). *J Exp Med.* 1997;185(12):2089-94.

39. Tough DF, Borrow P, and Sprent J. Induction of bystander T cell proliferation by viruses and type I interferon in vivo. *Science.* 1996;272(5270):1947-50.

40. de Jong AJ, Kloppenburg M, Toes RE, and Ioan-Facsinay A. Fatty acids, lipid mediators, and T-cell function. *Front Immunol.* 2014;5:483.

41. Vyas KS, and Wong LK. Detection of Biofilm in Wounds as an Early Indicator for Risk for Tissue Infection and Wound Chronicity. *Ann Plast Surg.* 2016;76(1):127-31.

42. Roy S, Elgharably H, Sinha M, Ganesh K, Chaney S, Mann E, et al. Mixed-species biofilm compromises wound healing by disrupting epidermal barrier function. *J Pathol.* 2014;233(4):331-43.

43. Rhoads DD, Cox SB, Rees EJ, Sun Y, and Wolcott RD. Clinical identification of bacteria in human chronic wound infections: culturing vs. 16S ribosomal DNA sequencing. *BMC Infect Dis.* 2012;12:321.

44. Niu M, and Keller NP. Co-opting oxylipin signals in microbial disease. *Cell Microbiol.* 2019;21(6):e13025.

45. Vance RE, Hong S, Gronert K, Serhan CN, and Mekalanos JJ. The opportunistic pathogen Pseudomonas aeruginosa carries a secretable arachidonate 15-lipoxygenase. *Proc Natl Acad Sci U S A.* 2004;101(7):2135-9.

46. Levan SR, Stamnes KA, Lin DL, Panzer AR, Fukui E, McCauley K, et al. Elevated faecal 12,13-diHOME concentration in neonates at high risk for asthma is produced by gut bacteria and impedes immune tolerance. *Nat Microbiol.* 2019;4(11):1851-61.

47. Kuo TM, Huang JK, Labeda D, Wen L, and Knothe G. Production of 10-hydroxy-8(E)-octadecenoic acid from oleic acid conversion by strains of Pseudomonas aeruginosa. *Curr Microbiol.* 2008;57(5):437-41.

48. Martinez E, and Campos-Gomez J. Oxylipins produced by Pseudomonas aeruginosa promote biofilm formation and virulence. *Nat Commun.* 2016;7:13823.
49. Levan SR, Stamnes KA, Lin DL, Fujimura KE, Ownby DR, Zoratti EM, et al. Neonatal gut-microbiome-derived 12,13 DiHOME impedes tolerance and promotes childhood atopy and asthma. *bioRxiv.* 2018:311704.
50. Perera LP, Zhang M, Nakagawa M, Petrus MN, Maeda M, Kadin ME, et al. Chimeric antigen receptor modified T cells that target chemokine receptor CCR4 as a therapeutic modality for T-cell malignancies. *Am J Hematol.* 2017;92(9):892-901.
51. Oishi N, Hundal T, Phillips JL, Dasari S, Hu G, Viswanatha DS, et al. Molecular profiling reveals a hypoxia signature in breast implant-associated anaplastic large cell lymphoma. *Haematologica.* 2020.
52. Yeung J, Adili R, Yamaguchi A, Freedman CJ, Chen A, Shami R, et al. Omega-6 DPA and its 12-lipoxygenase-oxidized lipids regulate platelet reactivity in a nongenomic PPARalpha-dependent manner. *Blood Adv.* 2020;4(18):4522-37.
53. Underhill DM, Bassetti M, Rudensky A, and Aderem A. Dynamic interactions of macrophages with T cells during antigen presentation. *J Exp Med.* 1999;190(12):1909-14.
54. Wells AF, Daniels S, Gunasekaran S, and Wells KE. Local increase in hyaluronic acid and interleukin-2 in the capsules surrounding silicone breast implants. *Ann Plast Surg.* 1994;33(1):1-5.
55. Parsonnet J. Bacterial infection as a cause of cancer. *Environ Health Perspect.* 1995;103 Suppl 8:263-8.
56. Tomkovich S, Yang Y, Winglee K, Gauthier J, Muhlbauer M, Sun X, et al. Locoregional Effects of Microbiota in a Preclinical Model of Colon Carcinogenesis. *Cancer Res.* 2017;77(10):2620-32.

57. Cappelli G, Tetta C, and Canaud B. Is biofilm a cause of silent chronic inflammation in haemodialysis patients? A fascinating working hypothesis. *Nephrol Dial Transplant.* 2005;20(2):266-70.

58. Hu H, Johani K, Almatroudi A, Vickery K, Van Natta B, Kadin ME, et al. Bacterial Biofilm Infection Detected in Breast Implant-Associated Anaplastic Large-Cell Lymphoma. *Plast Reconstr Surg.* 2016;137(6):1659-69.

59. Barki KG, Das A, Dixith S, Ghatak PD, Mathew-Steiner S, Schwab E, et al. Electric Field Based Dressing Disrupts Mixed-Species Bacterial Biofilm Infection and Restores Functional Wound Healing. *Ann Surg.* 2019;269(4):756-66.

60. Roy S, Santra S, Das A, Dixith S, Sinha M, Ghatak S, et al. Staphylococcus aureus Biofilm Infection Compromises Wound Healing by Causing Deficiencies in Granulation Tissue Collagen. *Ann Surg.* 2020;271(6):1174-85.

61. Sinha M, Ghosh N, Wijesinghe DS, Mathew-Steiner S, Das A, Singh K, et al. Pseudomonas aeruginosa Theft Biofilm Require Host Lipids of Cutaneous Wound. *Ann Surg.* 2021;in press(doi: 10.1097/SLA.0000000000005252).

62. James GA, Boegli L, Hancock J, Bowersock L, Parker A, and Kinney BM. Bacterial Adhesion and Biofilm Formation on Textured Breast Implant Shell Materials. *Aesthetic Plast Surg.* 2019;43(2):490-7.

63. Brandwein M, Steinberg D, and Meshner S. Microbial biofilms and the human skin microbiome. *NPJ Biofilms Microbiomes.* 2016;2:3.

64. Lee M, Ponraja G, McLeod K, and Chong S. Breast Implant Illness: A Biofilm Hypothesis. *Plast Reconstr Surg Glob Open.* 2020;8(4):e2755.

65. Glicksman CA. Implant Shell Characteristics: The Science Behind the Surface. *Clin Plast Surg.* 2021;48(1):79-86.

66. A KG, and Graf R. Breast Implant-Associated Anaplastic Large Cell Lymphoma (BIA-ALCL) and the Textured Breast Implant Crisis. *Aesthetic Plast Surg.* 2020;44(1):1-12.

67. Metzinger SE, Homsy C, Chun MJ, and Metzinger RC. Breast Implant Illness: Treatment Using Total Capsulectomy and Implant Removal. *Eplasty.* 2022;22:e5.
68. Katsnelson JY, Spaniol JR, Buinewicz JC, Ramsey FV, and Buinewicz BR. Outcomes of Implant Removal and Capsulectomy for Breast Implant Illness in 248 Patients. *Plast Reconstr Surg Glob Open.* 2021;9(9):e3813.
69. Toledo A, and Benach JL. Hijacking and Use of Host Lipids by Intracellular Pathogens. *Microbiol Spectr.* 2015;3(6).
70. Zhu ZR, Agren J, Mannisto S, Pietinen P, Eskelinen M, Syrjanen K, et al. Fatty acid composition of breast adipose tissue in breast cancer patients and in patients with benign breast disease. *Nutr Cancer.* 1995;24(2):151-60.
71. Gonzalez JF, Hahn MM, and Gunn JS. Chronic biofilm-based infections: skewing of the immune response. *Pathog Dis.* 2018;76(3).
72. Liblau RS, Singer SM, and McDevitt HO. Th1 and Th2 CD4+ T cells in the pathogenesis of organ-specific autoimmune diseases. *Immunol Today.* 1995;16(1):34-8.
73. Pastar I, O'Neill K, Padula L, Head CR, Burgess JL, Chen V, et al. Staphylococcus epidermidis Boosts Innate Immune Response by Activation of Gamma Delta T Cells and Induction of Perforin-2 in Human Skin (vol 11, 550946, 2020). *Frontiers in Immunology.* 2021;12.
74. Leonel C, Sena IFG, Silva WN, Prazeres P, Fernandes GR, Mancha Agresti P, et al. Staphylococcus epidermidis role in the skin microenvironment. *J Cell Mol Med.* 2019;23(9):5949-55.
75. Merana GR, Dwyer LR, Dhariwala MO, Weckel A, Gonzalez JR, Okoro JN, et al. Intestinal inflammation alters the antigen-specific immune response to a skin commensal. *Cell Rep.* 2022;39(9):110891.
76. Calder PC, and Harris WS. Lipids to support physiology and function: both quantity and quality are important. *Curr Opin Clin Nutr.* 2023;26(3):273-7.

77. Kabashima K, Sakata D, Nagamachi M, Miyachi Y, Inaba K, and Narumiya S. Prostaglandin E2-EP4 signaling initiates skin immune responses by promoting migration and maturation of Langerhans cells. *Nat Med.* 2003;9(6):744-9.
78. Jo-Watanabe A, Okuno T, and Yokomizo T. The Role of Leukotrienes as Potential Therapeutic Targets in Allergic Disorders. *Int J Mol Sci.* 2019;20(14).
79. Xue L, Barrow A, Fleming VM, Hunter MG, Ogg G, Klenerman P, et al. Leukotriene E4 activates human Th2 cells for exaggerated proinflammatory cytokine production in response to prostaglandin D2. *J Immunol.* 2012;188(2):694-702.
80. Jackson CD, Hilliard KA, and Brown CR. 12/15-lipoxygenase activity promotes efficient inflammation resolution in a murine model of Lyme arthritis. *Frontiers in Immunology.* 2023;14.
81. Sousa AB, and Barbosa JN. The Use of Specialized Pro-Resolving Mediators in Biomaterial-Based Immunomodulation. *J Funct Biomater.* 2023;14(4).
82. Osthues T, and Sisignano M. Oxidized Lipids in Persistent Pain States. *Front Pharmacol.* 2019;10:1147.

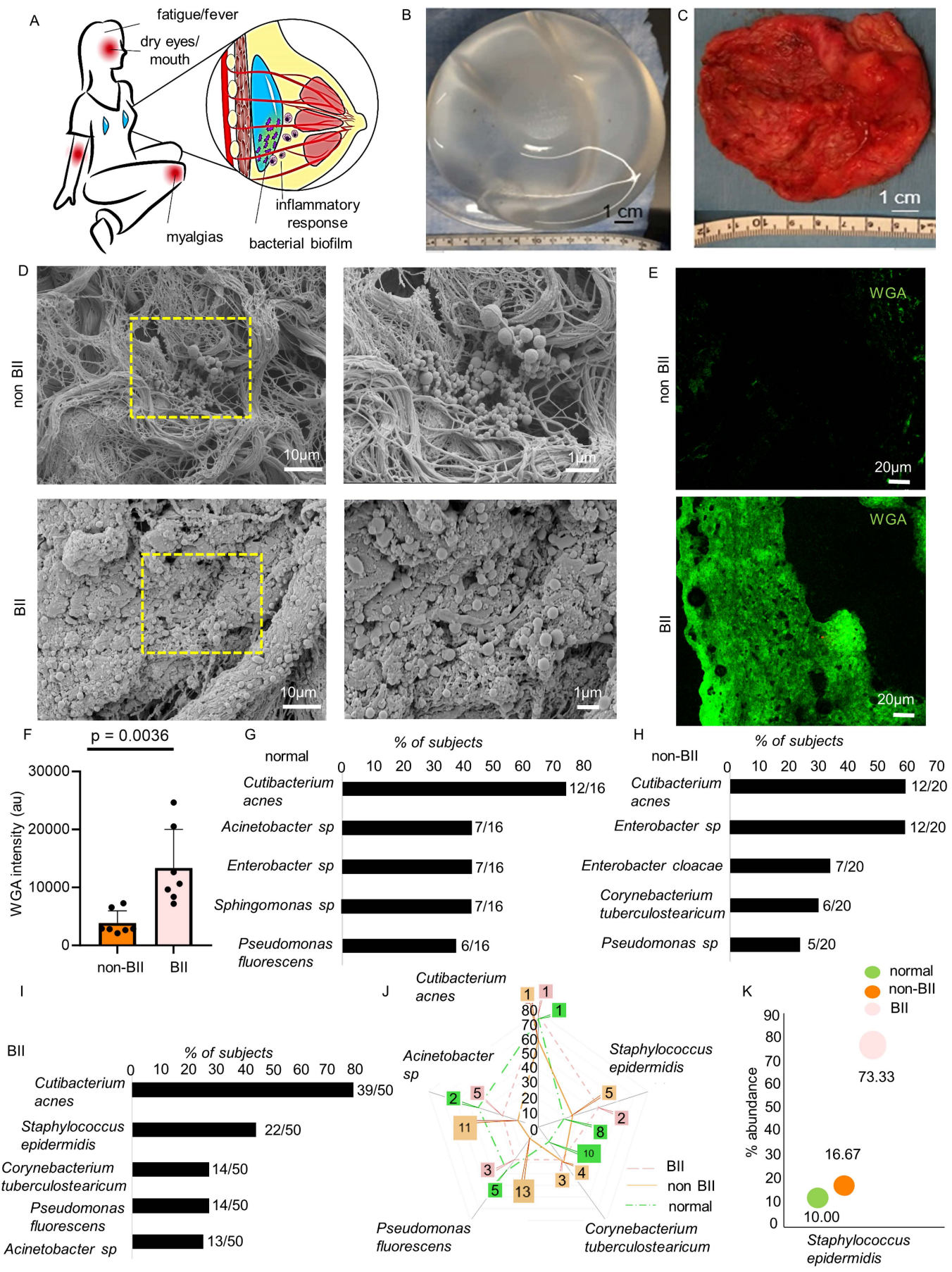
A
fatigue/fever
dry eyes/
mouth
myalgias
inflammatory
response
bacterial biofilm
B
1 cm
C
1 cm
D
non BII
BII
10μm
1μm
E
non BII
BII
WGA
20μm
F
p = 0.0036
WGA intensity (au)
30000
20000
10000
0
non-BII
BII
G
normal
% of subjects
0 10 20 30 40 50 60 70 80
Cutibacterium acnes 12/16
Acinetobacter sp 7/16
Enterobacter sp 7/16
Sphingomonas sp 7/16
Pseudomonas fluorescens 6/16
H
non-BII
% of subjects
0 10 20 30 40 50 60 70
Cutibacterium acnes 12/20
Enterobacter sp 12/20
Enterobacter cloacae 7/20
Corynebacterium tuberculostearicum 6/20
Pseudomonas sp 5/20
I
BII
% of subjects
0 10 20 30 40 50 60 70 80
Cutibacterium acnes 39/50
Staphylococcus epidermidis 22/50
Corynebacterium tuberculostearicum 14/50
Pseudomonas fluorescens 14/50
Acinetobacter sp 13/50
J
Cutibacterium acnes
Staphylococcus epidermidis
Corynebacterium tuberculostearicum
Pseudomonas fluorescens
Acinetobacter sp
BII
non BII
normal
K
normal
non-BII
BII
% abundance
90
80
70
60
50
40
30
20
10
0
73.33
16.67
10.00
Staphylococcus epidermidis

Figure 1. Bacterial Biofilm in Implant-Associated with BII

(A) Schematic presentation of the bacterial biofilm association with breast implant illness (BII)

(B) Breast implant isolated from a subject.

(C) Capsule associated with breast implant of the subject shown in panel (B).

(D) Increased abundance of bacterial biofilm from the implant-associated capsule of BII compared to non-BII subjects as determined through scanning electron microscopy. Zoomed insets of region of interest (ROI) dotted yellow square shown. n=10 (non-BII), n=25 (BII) subjects.

(E-F) E, Increased abundance of bacterial biofilm as measured through wheat germ agglutinin (WGA) assay in the capsules of BII subjects compared to the non-BII capsules. **F**, Quantification of biofilm aggregates using WGA staining. Data presented as mean ± SEM, n=7 (non-BII), n=7 (BII) subjects. t test BII *vs* non-BII (p=0.0036).

(G-I) 16S rRNA NGS-based bacterial typing from the breast tissues of **G**, normal; **H**, non-BII, and **I**, BII subjects. Top five bacterial species in each group represented. Fraction of subject samples associated with a bacterial species is provided in parenthesis n=16 (normal), n=20 (non-BII), n=50 (BII).

(J) Spider-plot depicting the ranking of the top 5 bacterial infection types in the BII group compared to their ranking in the non-BII and normal groups. The intersection of the group lines with the spikes of the spider-plot indicates the proportion of these infections by groups. The call out numbers are the ranks for each of these infections within each group. n=16 (normal), n=20 (non-BII), n=50 (BII).

(K) Increased abundance of biofilm forming *Staphylococcus epidermidis* in implant-associated breast tissues of BII subjects. Bubble plot indicating the percentage of patients with *Staphylococcus epidermidis* provided above the individual bars. The bubble percentage indicate the likelihood of a subject with *S. epidermidis* biofilm in each of the three groups. n=16 (normal), n=20 (non-BII), n=50 (BII) subjects.

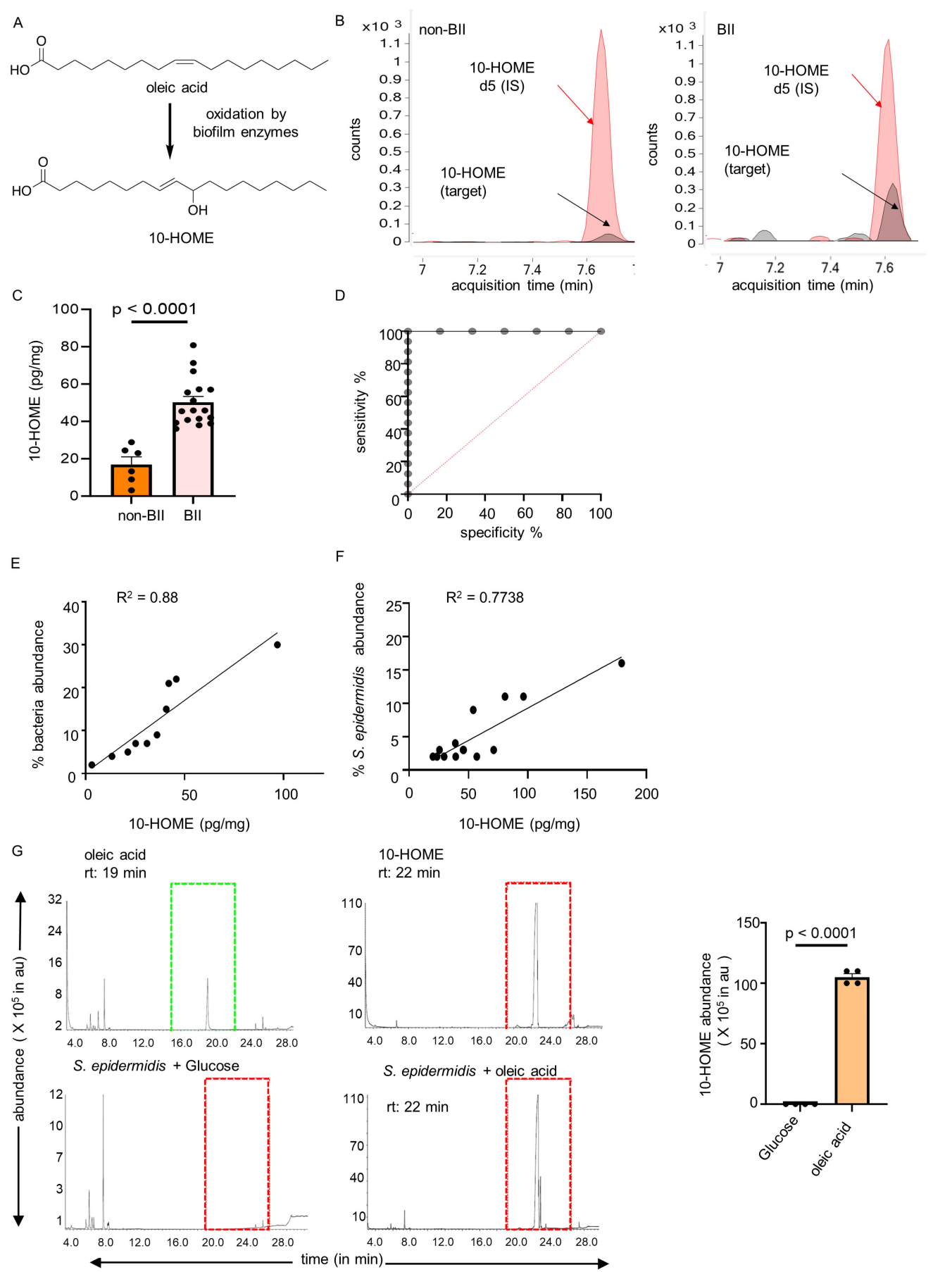
A
oleic acid
oxidation by biofilm enzymes
10-HOME
B
non-BII
BII
10-HOME d5 (IS)
10-HOME (target)
counts
acquisition time (min)
C
p < 0.0001
10-HOME (pg/mg)
non-BII
BII
D
sensitivity %
specificity %
E
R2 = 0.88
% bacteria abundance
10-HOME (pg/mg)
F
R2 = 0.7738
% S. epidermidis abundance
10-HOME (pg/mg)
G
oleic acid
rt: 19 min
10-HOME
rt: 22 min
S. epidermidis + Glucose
S. epidermidis + oleic acid
rt: 22 min
abundance (X 10^5 in au)
time (in min)
10-HOME abundance (X 10^5 in au)
p < 0.0001
Glucose
oleic acid

Figure 2. Increased Abundance of Biofilm-Derived 10-HOME in BII Subjects

(A) Schematic of formation of (*E*)-10-hydroxy-8-octadecenoic acid (10-HOME) from oleic acid.

(B-D) Increased abundance of 10-HOME in implant-associated tissue of BII subjects. **B**.

Chromatograms of 10-HOME from non-BII and BII using LC-MS/MS targeted analyses. **C**. Data

presented as mean ± SEM, n=6 (non-BII), n=17 (BII), t test BII *vs* non-BII ($p<0.0001$).. **D**. Receiver operating characteristic (ROC) curve analysis to determine specificity and sensitivity of 10-HOME detection.

(E) Increased abundance of bacteria associated with 10-HOME detected from the implant-associated tissue of BII subjects.

(F) Increased abundance of *Staphylococcus epidermidis* associated with 10-HOME detected from the implant-associated tissue of BII subjects.

(G) Synthesis of 10-HOME by *S. epidermidis in vitro* upon using oleic acid as carbon source. Gas chromatography-mass spectrometry analyses for detection of 10-HOME derivatized both as trimethylsilyl ethers and methyl estersoleic acid standard, 10-HOME standard, *S. epidermidis* with glucose as carbon source, *S. epidermidis* with oleic acid as carbon source, quantification of 10-HOME abundance. n=4. t test glucose *vs* oleic acid ($p<0.0001$).

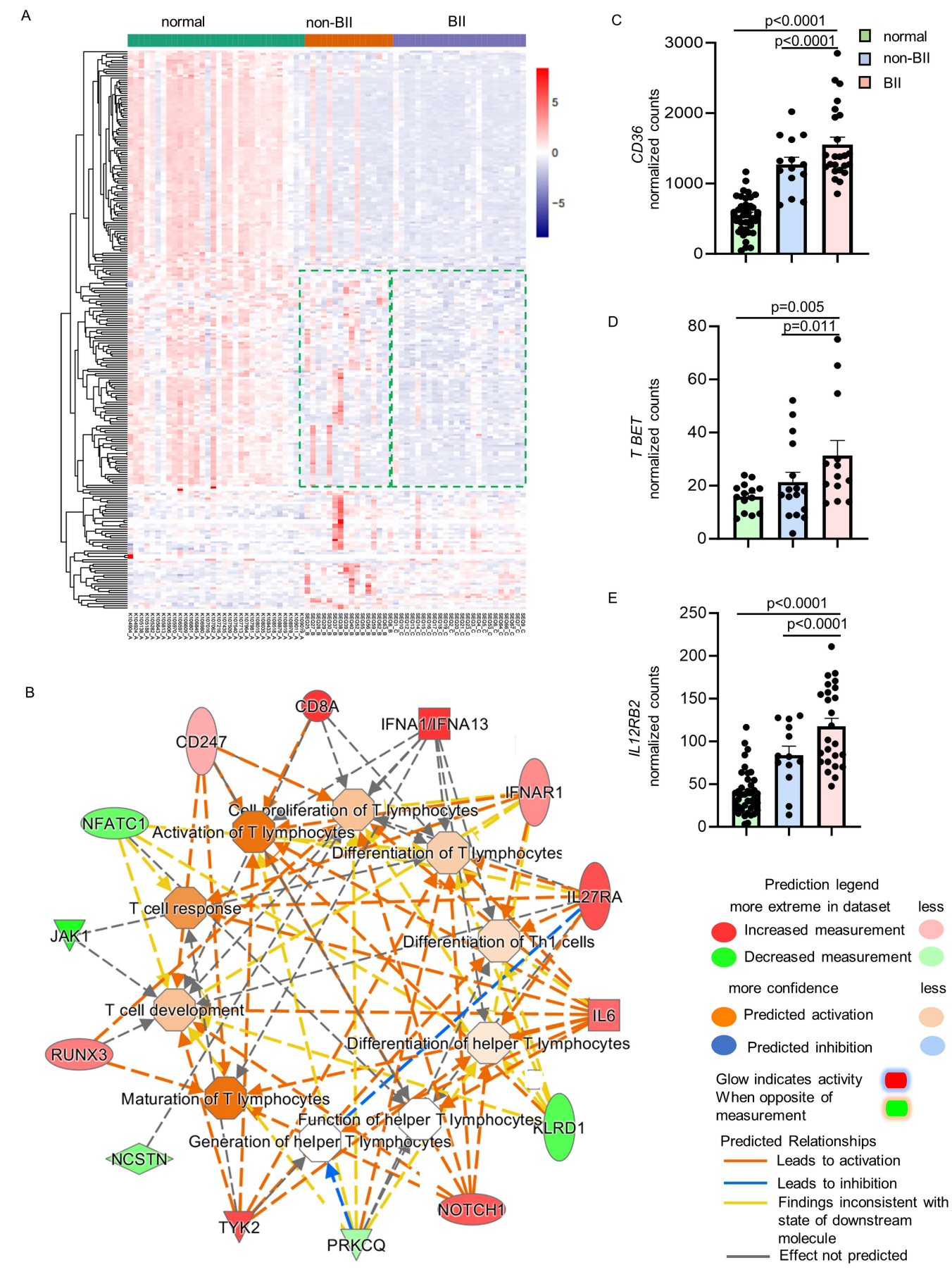
A
normal
non-BII
BII
5
0
−5
B
CD8A
CD247
IFNA1/IFNA13
IFNAR1
Cell proliferation of T lymphocytes
NFATC1
Activation of T lymphocytes
Differentiation of T lymphocytes
IL27RA
T cell response
JAK1
Differentiation of Th1 cells
T cell development
IL6
RUNX3
Differentiation of helper T lymphocytes
Maturation of T lymphocytes
Function of helper T lymphocytes
KLRD1
Generation of helper T lymphocytes
NCSTN
NOTCH1
TYK2
PRKCQ
C
p<0.0001
p<0.0001
normal
non-BII
BII
CD36
normalized counts
3000
2000
1000
0
D
p=0.005
p=0.011
T BET
normalized counts
80
60
40
20
0
E
p<0.0001
p<0.0001
IL12RB2
normalized counts
250
200
150
100
50
0
Prediction legend
more extreme in dataset
less
Increased measurement
Decreased measurement
more confidence
less
Predicted activation
Predicted inhibition
Glow indicates activity
When opposite of
measurement
Predicted Relationships
Leads to activation
Leads to inhibition
Findings inconsistent with
state of downstream
molecule
Effect not predicted

Figure 3. Comparative Transcriptomic and Molecular Pathway Analyses of BII Subjects

(A) Hierarchical clustering of genes with at least 2-fold change and controlled by false discovery rate (FDR) of 0.05 breast tissue from normal (n=34), non-BII (n=16) and BII (n=24) subjects.

(B) Gene interaction networks for functions related to differentiation of T-lymphocytes, differentiation of Th1 cells, cell proliferation of T-lymphocytes, maturation of T-lymphocytes, generation of T-helper lymphocytes, differentiation of helper T-lymphocytes, T-cell response, T-cell development, quantity of T-lymphocytes in BII specimens. Represented functional networks relevant to the set of imported genes generated by Canonical Pathway function relevant to Th1 pathway. The list was selected from the hierarchical cluster of Th1 genes, that were upregulated are shown in red and downregulated in green. The intensity of red and green corresponds to an increase and decrease, respectively, in log2 fold change.

(C) Comparison of normalized RNA-Seq counts for *CD36* between normal, non-BII and BII samples. In an age-adjusted nonparametric regression model, compared to normal subjects, normalized number of *CD36* counts was approximately 1116 units higher in the BII group ($p<0.0001$) and 650 units higher in the non-BII group ($p<0.0001$).

(D) Comparison of normalized RNA-Seq counts for Th1 gene *T-BET (TXB21)* between normal, non-BII and BII samples. In an age-adjusted nonparametric regression model, compared to normal subjects, the normalized number of *T-BET* counts was approximately 18 units higher in the BII group ($p=0.005$) and 11 units higher in the non-BII group ($p=0.011$).

(E) Comparison of normalized RNA-Seq counts forTh1 gene *IL12RB2* between normal, non-BII and BII samples. In an age-adjusted nonparametric regression model, compared to normal subjects, the normalized number of *IL12RB2* counts was approximately 84 units higher in the BII group ($p<0.0001$) and 45 units higher in the non-BII group ($p<0.0001$).

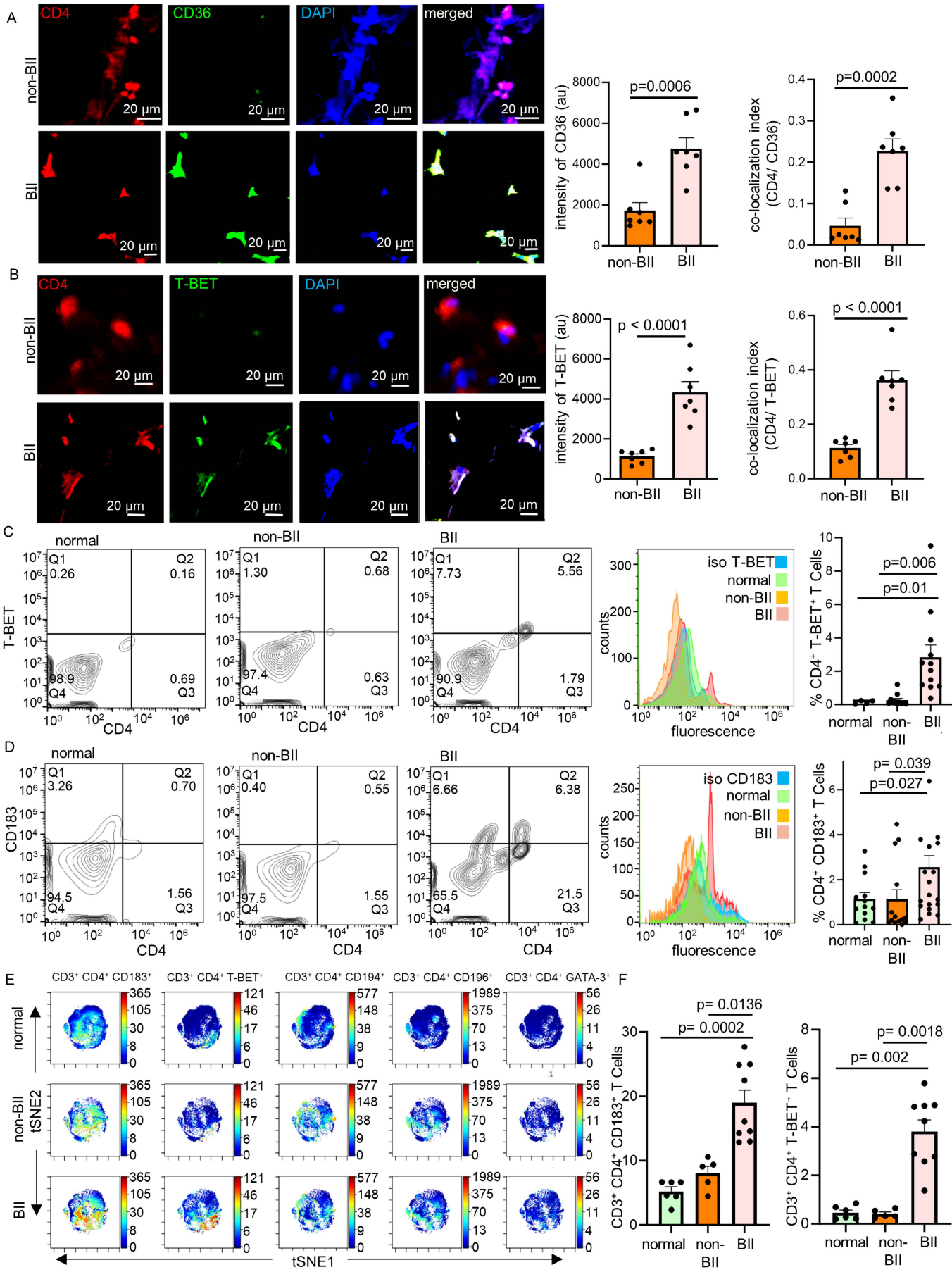
A
CD4
CD36
DAPI
merged
non-BII
BII
20 μm
intensity of CD36 (au)
p=0.0006
co-localization index (CD4/ CD36)
p=0.0002
B
T-BET
intensity of T-BET (au)
p < 0.0001
co-localization index (CD4/ T-BET)
C
normal
non-BII
BII
T-BET
CD4
Q1 0.26
Q2 0.16
Q4 98.9
Q3 0.69
Q1 1.30
Q2 0.68
Q4 97.4
Q3 0.63
Q1 7.73
Q2 5.56
Q4 90.9
Q3 1.79
iso T-BET
counts
fluorescence
% CD4+ T-BET+ T Cells
p=0.006
p=0.01
D
CD183
Q1 3.26
Q2 0.70
Q4 94.5
Q3 1.56
Q1 0.40
Q2 0.55
Q4 97.5
Q3 1.55
Q1 6.66
Q2 6.38
Q4 65.5
Q3 21.5
iso CD183
% CD4+ CD183+ T Cells
p= 0.039
p=0.027
E
CD3+ CD4+ CD183+
CD3+ CD4+ T-BET+
CD3+ CD4+ CD194+
CD3+ CD4+ CD196+
CD3+ CD4+ GATA-3+
tSNE2
tSNE1
F
CD3+ CD4+ CD183+ T Cells
p= 0.0136
p= 0.0002
CD3+ CD4+ T-BET+ T Cells
p= 0.0018
p= 0.002

Figure 4. Abundance of $CD4^+$ Th1 Cells in Implant Associated Tissue of BII Subjects

(A) Increased expression of CD36 in breast tissue associated with BII subjects, immunostained with anti-CD4(red), anti-CD36(green) and DAPI(blue). Data presented as mean ± SEM, (n=7). Scale bar = 20 μm. t test BII *vs* non-BII Intensity (p=0.0006), co-localization (p=0.0002).

(B) Increased expression of T-BET in breast tissue associated with BII subjects, immunostained with anti-CD4(red), anti-T-BET(green) and DAPI(blue). Data presented as mean ± SEM, (n=7). Scale bar = 20 μm. t test BII *vs* non-BII Intensity($p<0.0001$), co-localization($p<0.0001$).

(C) Flow cytometry with anti-CD4 (FITC) and anti-TBET (PE). Representative plots: normal, BII, histogram with isotype control for T-BET. Data presented as mean ± SEM, n= 4 (normal), n=11 (non-BII), n=12(BII). Bivariate Kruskal-Wallis with post-hoc Benjamini-Hochberg adjusted pairwise comparison analysis BII *vs* normal(p=0.01); BII *vs* non-BII(p=0.006).

(D) Elevated Th1 subtype in the peripheral blood of BII subjects. Flow cytometry analyses

peripheral blood of subjects stained with anti-CD4(FITC) and anti-CD183(PE). Representative flow plots: normal, non-BII, BII, histogram with isotype control for CD183. Data presented as mean ± SEM, n=13 (normal), n=14 (non-BII), n=20 (BII). Bivariate Kruskal- Wallis with post-hoc Benjamini-Hochberg adjusted pairwise comparison analysis BII *vs* normal (p=0.027); BII *vs* non-BII (p=0.039).

(E) Representative viSNE plots for $CD3^+$ $CD4^+$ T cells. Color depicts the intensity of the marker labeled on arcsinh scales from blue (low) to red (high). The analyses indicated elevated Th1 subtype in the peripheral blood of BII subjects.

(**F**) Quantification of median marker expression using CytoBank software for panel **E,** CD183 and T-BET, n=6 (normal), n=5 (non-BII), n=9 (BII). Bivariate Kruskal-Wallis with post-hoc Benjamini-Hochberg adjusted pairwise comparison analysis. For CD183, BII *vs* normal (p=0.0002); BII vs non-BII (p=0.0136). For T-BET, BII *vs* normal (p=0.002); BII *vs* non-BII (p=0.0018). The quantification of remainder viSNE plots in **Supplementary Fig S15**.

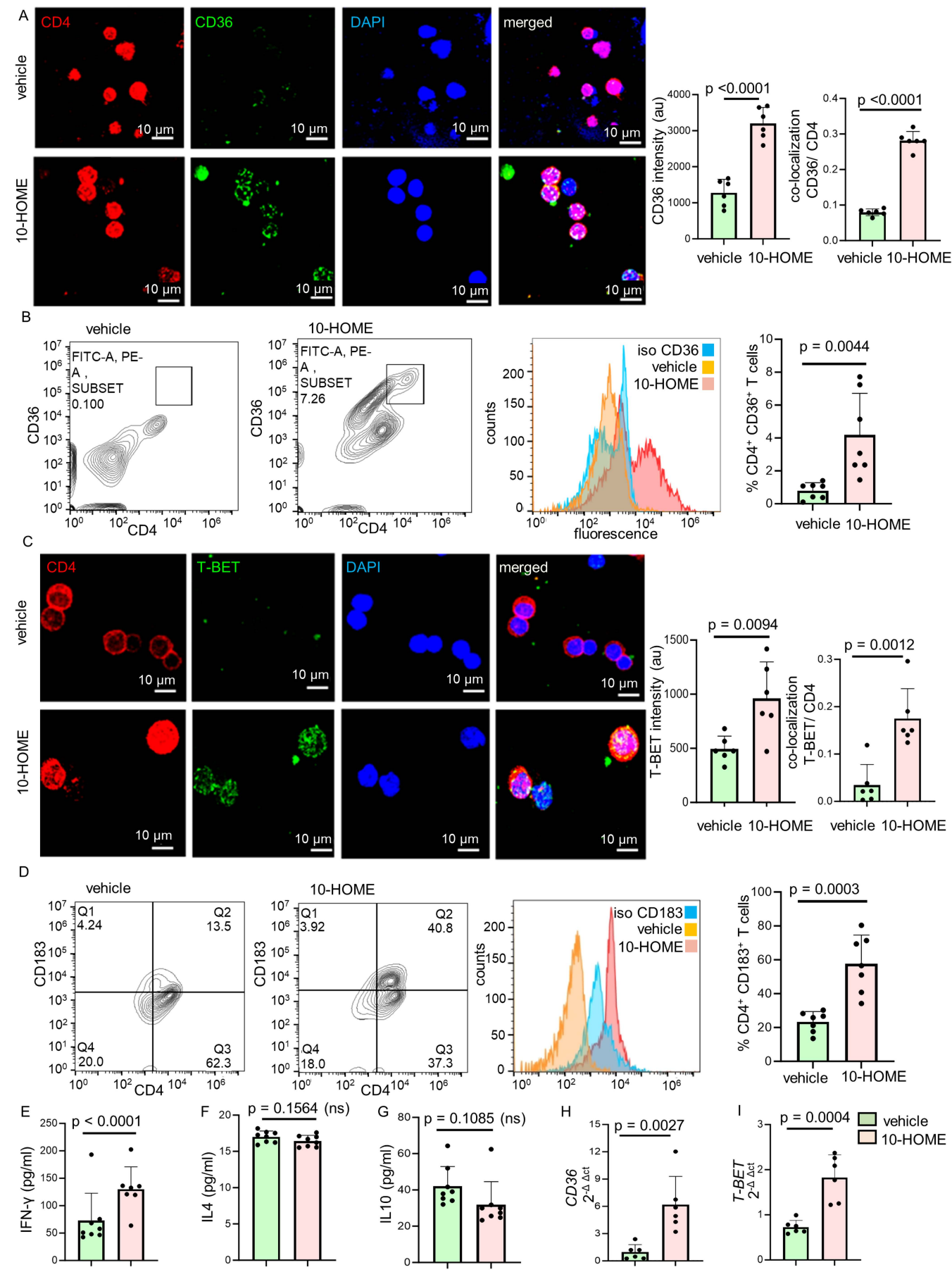
A
CD4
CD36
DAPI
merged
vehicle
10-HOME
10 µm
CD36 intensity (au)
p <0.0001
co-localization CD36/ CD4
p <0.0001
vehicle
10-HOME
B
vehicle
10-HOME
FITC-A, PE-A , SUBSET 0.100
FITC-A, PE-A , SUBSET 7.26
CD36
CD4
counts
fluorescence
iso CD36
vehicle
10-HOME
% CD4+ CD36+ T cells
p = 0.0044
C
CD4
T-BET
DAPI
merged
T-BET intensity (au)
p = 0.0094
co-localization T-BET/ CD4
p = 0.0012
D
Q1 4.24
Q2 13.5
Q4 20.0
Q3 62.3
Q1 3.92
Q2 40.8
Q4 18.0
Q3 37.3
CD183
iso CD183
% CD4+ CD183+ T cells
p = 0.0003
E
IFN-γ (pg/ml)
p < 0.0001
F
IL4 (pg/ml)
p = 0.1564 (ns)
G
IL10 (pg/ml)
p = 0.1085 (ns)
H
CD36 2-Δ Δct
p = 0.0027
I
T-BET 2-Δ Δct
p = 0.0004

Figure 5. Oxylipin 10-HOME Polarizes Naïve CD4$^+$ T Cells to Th1 Subtype *in vitro*

(A) Increased expression of CD36 in naïve CD4$^+$ T cells treated with 10-HOME immunostained with anti-CD4 (red), anti-CD36 (green) and DAPI (blue). Intensity of CD36. Colocalization of CD4 and CD36 depicted increased abundance of CD4$^+$ CD36$^+$ cells. Data presented as mean ± SD, (n=6). Scale bar = 10 μm. t test vehicle *vs* 10-HOME, intensity($p<0.0001$), co-localization($p<0.0001$).

(B) Elevated CD36 in the 10-HOME treated naïve T cells. Flow cytometry analyses of treated cells stained with anti-CD4(FITC) and anti-CD36(APC). Representative plots: vehicle,10-HOME-treated cells,histograms of with isotype control for CD36. Data presented as mean ± SD, (n=7). t test vehicle *vs* 10-HOME($p=0.0044$).

(C) Increased expression of T-BET in the 10-HOME treated naïve CD4$^+$ T cells immunostained with anti-CD4(red), anti-TBET(green) and DAPI(blue). Intensity of TBET quantified. Colocalization of CD4 and TBET depicted increased abundance of CD4$^+$ TBET$^+$ cells. Data presented as mean ± SD, (n=6). Scale bar = 10 μm. t test vehicle *vs* 10-HOME Intensity($p=0.0094$), co-localization($p=0.0012$).

(D) Elevated Th1 subtype (CD183$^+$) in the 10-HOME treated naïve CD4$^+$ T cells. Flow cytometry analyses with anti-CD4(FITC) and anti-CD183(PE). Representative plots: vehicle-treated,10-HOME-treated cells,histograms of cells with isotype control for CD183. Data presented as mean ± SD, (n=7). t test vehicle *vs* 10-HOME Intensity($p=0.0094$), co-localization($p=0.0003$).

(E) Increased expression of IFN-γ in the 10-HOME treated naïve CD4$^+$ T cells as measured through ELISA. Data presented as mean ± SD (n=7). t test vehicle *vs* 10-HOME Intensity($p=0.0094$), co-localization($p<0.0001$).

(F-G) No significant change in IL4 and IL10 following 10-HOME treatment of naïve CD4$^+$ T cells. Data presented as mean ± SD, (n=8). t test vehicle *vs* 10-HOME, 1L4($p=0.1564$), IL10($p=0.1085$).

(H-I) Increased expression of (**H**) *CD36* (**I**) *T-BET* in 10-HOME-treated naïve T cells. Data presented as mean ± SD, (n=6). t test vehicle *vs* 10-HOME *CD36*($p=0.0027$), *T-BET*($p=0.0004$).

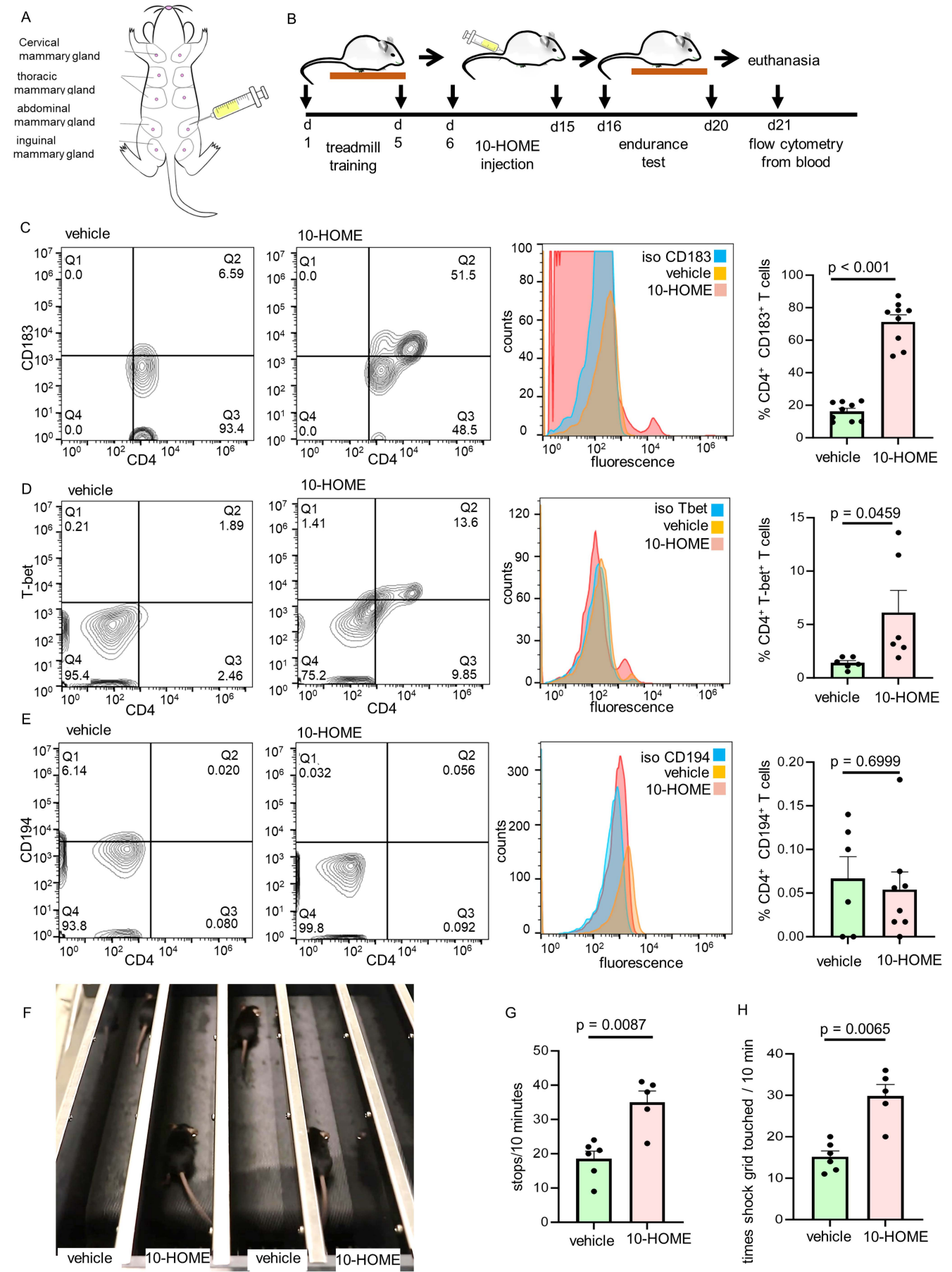
A
Cervical mammary gland
thoracic mammary gland
abdominal mammary gland
inguinal mammary gland
B
euthanasia
d 1
treadmill training
d 5
d 6
10-HOME injection
d15
d16
endurance test
d20
d21
flow cytometry from blood
C
vehicle
10-HOME
CD183
CD4
Q1 0.0
Q2 6.59
Q4 0.0
Q3 93.4
Q1 0.0
Q2 51.5
Q4 0.0
Q3 48.5
iso CD183
vehicle
10-HOME
counts
fluorescence
p < 0.001
% CD4+ CD183+ T cells
D
T-bet
Q1 0.21
Q2 1.89
Q4 95.4
Q3 2.46
Q1 1.41
Q2 13.6
Q4 75.2
Q3 9.85
iso Tbet
p = 0.0459
% CD4+ T-bet+ T cells
E
CD194
Q1 6.14
Q2 0.020
Q4 93.8
Q3 0.080
Q1 0.032
Q2 0.056
Q4 99.8
Q3 0.092
iso CD194
p = 0.6999
% CD4+ CD194+ T cells
F
vehicle
10-HOME
vehicle
10-HOME
G
p = 0.0087
stops/10 minutes
H
p = 0.0065
times shock grid touched / 10 min

Figure 6. Elevated $CD4^+$ Th1 and Fatigue-like Symptoms in Mice Administered with 10-HOME

(A) Schematic representation of injection of 10-HOME in the abdominal mammary fat pad of mice.

(B) Timeline of 10-HOME administration in mice.

(C) Elevated $CD4^+$ Th1 subtype in the blood of mice injected with 10-HOME. Flow cytometry analyses of blood of mice stained with anti-CD4 (FITC) and anti-CD183 (PE). Representative flow plots. Vehicle-treated, 10-HOME-treated, histograms with isotype control for CD183 . Data presented as mean ± SEM, vehicle (n=9) and 10-HOME (n=9) mice. Wilcoxon-Rank test analysis vehicle *vs* 10-HOME ($p<0.001$).

(D) Elevated $CD4^+$ Th1 subtype in the blood of mice injected with 10-HOME. Flow cytometry analyses of blood of mice stained with anti-CD4 (FITC) and anti-Tbet (PE). Representative flow plots. Vehicle-treated 10-HOME-treated histograms with isotype control for T-bet. Data presented as mean ± SEM, vehicle (n=6) and 10-HOME (n=6) mice. t test vehicle vs 10-HOME($p = 0.0459$)

(E) Unaltered $CD4^+$ Th2 subtype in the blood of mice injected with 10-HOME. Flow cytometry analyses of blood of mice stained with anti-CD4 (FITC) and anti-CD194 (PE). Representative flow plots. Vehicle-treated 10-HOME-treated histograms with isotype control for CD194. Data presented as mean ± SEM, vehicle (n=6) and 10-HOME (n=8) mice. t test vehicle vs 10-HOME($p = 0.6999$)

(F) Representative image of murine endurance test post 10-HOME administration. Video provided as **Supplementary Video 1**.

(G) Increased stops exhibited by 10-HOME administered mice compared to those treated with vehicle. Data presented as mean ± SEM, vehicle (n=6) and 10-HOME (n=5) mice. Mann-Whitney U-test with a Bonferroni correction was performed ($p=0.0087$).

(H) Increased aversive stimulation (shock grid touching) exhibited by mice administered 10-HOME compared to those treated with vehicle. Data presented as mean ± SEM, vehicle (n=6) and 10-HOME (n=5) mice. Mann-Whitney U-test with a Bonferroni correction was performed ($p=0.0065$).

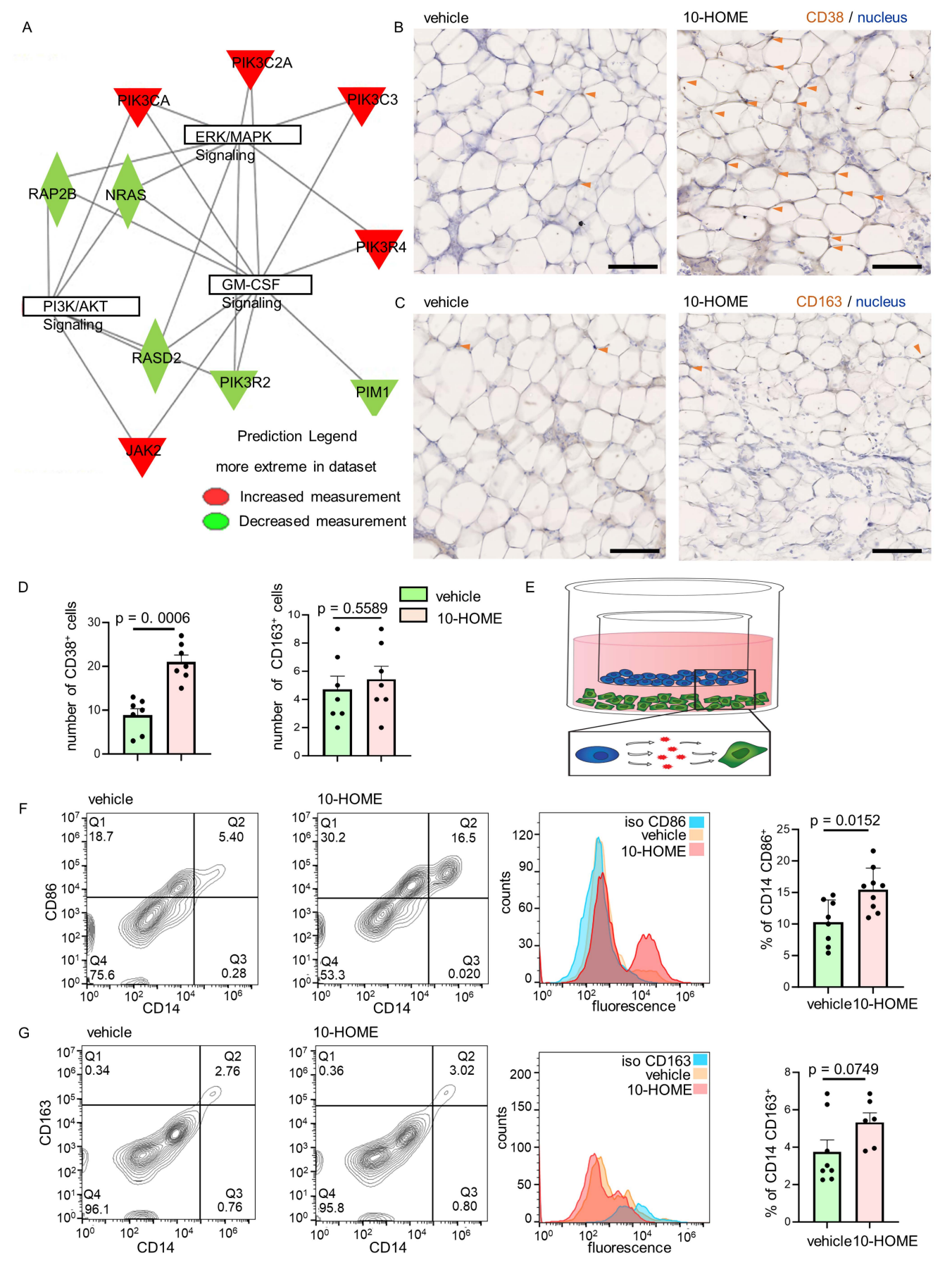
A
PIK3C2A
PIK3CA
PIK3C3
ERK/MAPK Signaling
RAP2B
NRAS
PIK3R4
GM-CSF Signaling
PI3K/AKT Signaling
RASD2
PIK3R2
PIM1
JAK2
Prediction Legend
more extreme in dataset
Increased measurement
Decreased measurement
B
vehicle
10-HOME
CD38 / nucleus
C
vehicle
10-HOME
CD163 / nucleus
D
number of CD38+ cells
p = 0. 0006
number of CD163+ cells
p = 0.5589
vehicle
10-HOME
E
F
vehicle
10-HOME
CD86
CD14
Q1 18.7
Q2 5.40
Q4 75.6
Q3 0.28
Q1 30.2
Q2 16.5
Q4 53.3
Q3 0.020
iso CD86
vehicle
10-HOME
counts
fluorescence
p = 0.0152
% of CD14 CD86+
G
vehicle
10-HOME
CD163
CD14
Q1 0.34
Q2 2.76
Q4 96.1
Q3 0.76
Q1 0.36
Q2 3.02
Q4 95.8
Q3 0.80
iso CD163
vehicle
10-HOME
counts
fluorescence
p = 0.0749
% of CD14 CD163+

Figure 7. CD4+ T Cells in Reaction with 10-HOME Polarizes Macrophages to M1 Phenotype.

(A) Gene interaction networks from human bulk RNA-Sequpregulated genes in red and downregulated are in green, in log2 fold change. Table exhibited in **Supplementary Figure S21A**.

(**B**) Increased expression of CD38 (M1 macrophage marker) in 10-HOME-treated mice compared to vehicle. Murine mammary fat pads stained with anti-CD38 antibody antibody(DAB) and nucleus(hematoxylin). The cells in adipose tissues are bordered by adipose cells. Cells co-expressing DAB and hematoxylin were considered (arrows). Data presented as mean ± SEM, vehicle (n=7) and 10-HOME (n=7) mice. Scale bar = 100μm. Enlarged image in **Supplementary Figure S22**.

(C) No significant difference of CD163 (M2 macrophage marker) in 10-HOME treated mice. Murine mammary fat pads stained with anti-CD38 antibody (DAB). Cells co-expressing DAB and hematoxylin were considered (arrows). Data presented as mean ± SEM, vehicle (n=7) and 10-HOME (n=7) mice. Scale bar = 100μm. Enlarged image in **Supplementary Figure S23**.

(D) Quantification of B-C. Total number of CD38+, CD163+ cells were calculated. Data presented as mean ± SEM, (n=7). Mann Whitney test vehicle *vs* 10-HOME CD38 (p=0.0006), CD163 (p=0.558).

(E) Schematic representation of macrophage- T cell trans-well assay. PBMC-derived naïve T cells treated with 10-HOME (blue), PBMC-derived M0 macrophages (green).

(F) Increased polarization to M1 phenotype (CD86-human M1 marker) in the trans-well co-culture of PBMC derived M0 macrophages incubated with10-HOME-treated naïve $CD4^+$ T cells. Flow cytometry analyses with anti-CD86(FITC) and anti-CD14(PE). Representative plots, vehicle treated,10-HOME treated, histograms of cells with isotype control for CD86. Data presented as mean ± SD, (n=8). Mann Whitney test comparison vehicle vs 10-HOME(p=0.0152).

(G) Unaltered M2 phenotype(CD163). Flow cytometry analyses with anti-CD163(APC) and anti-CD14(PE). Representative plots, vehicle treated,10-HOME-treated, histograms with isotype control for CD163. Data presented as mean ± SD, (n=8). Mann Whitney test vehicle *vs* 10-HOME (p=0.0749).